# IMPROVING CFD ANALYSIS OF DC FURNACE OPERATION BY REFINING AND ADDITION OF TRANSPORTATION PHENOMENA MODELS

**B. Henning, M. Shapiro[1] and L.A. le Grange[2]**

*Pyrometallurgy Technology, Bateman Minerals & Metals, South Africa*
*[1]Pyrometallurgy Technology, Bateman Minerals & Metals, South Africa*
*[2]CFD Software Developer, Flo++®, South Africa*
*E-mail: bennie.henning@batemanbv.com; mike.shapiro@batemanbv.com; louis.legr@softflo.com*

## ABSTRACT

*A paper was presented by Bateman Minerals and Metals at INFACONX (2004) describing a simplified Computational Fluid Dynamics (CFD) Model for predicting the temperature and velocity distributions in all the fluid zones of a single electrode DC Furnace simultaneously with the temperature distributions in the refractory lining of the vessel. The boundary conditions imposed on the model consisted of the arc current, external surface film coefficients and ambient temperatures. The temperature and velocity distributions in the freeboard, slag and metal were solved simultaneously by coupling across the interfaces between the fluids and transportation phenomena developing in the plasma arc. A simplified model was used to describe the exchange of energy by radiation between the arc and surfaces enclosing the freeboard region.*

*The strengths of this model were reported as being the ability to:*

- *Solve the different zones and transportation phenomena simultaneously without the need to transfer partial numerical results between different numerical analysis applications.*
- *Solve velocity and temperature distributions without assumptions regarding internal film coefficients and additional internal temperature boundary conditions.*

*One of the disadvantages of the model was that the energy absorbed by the process was not modelled, resulting in vessel performance predictions under heat loss conditions only. Whilst this allowed potential problem areas such as localized refractory heating to be identified, the model was only capable of predicting how these could be improved by varying the overall geometry and materials of construction.*

*This paper presents improvements in the application software and user defined subroutines of the model as follows:*

- *Incorporation of surface to gas, gas to gas and gas to surface radiation models to improve the accuracy of radiative heat transfer mechanisms within the freeboard.*
- *Incorporation of a process energy absorption model based on a theoretical temperature dependant enthalpy curve which incorporates melting, smelting and superheating in selected areas of the bath. This enables the effect of feed distribution and power to feed ratio changes to be estimated. The effects of a commercial arc at full power on the freeboard and slag can now be simulated with increased accuracy.*

## 1. INTRODUCTION

Bateman presented a paper on Arc-Bath modelling in DC furnaces using CFD at INFACON X. The work was carried out in association with Flo++®, who developed additional modules to solve the simplified MHD source terms, and surface to surface radiation energy transfer. A significant part of the work involved the development of suitable solution strategies to ensure numerical stability and convergence of the solution. The model presented at that conference predicts the temperature and velocity fields in the arc, freeboard, slag and metal regions of a DC Arc Furnace operating under heat loss conditions. The temperature in the refractory lining of the associated containment vessel is predicated using the conjugate heat transfer capabilities of the application software. It enabled the effect of varying operating parameters such as arc length at constant power (i.e. increased voltage and reduced current) on temperature distribution within the system to be predicted.

The model was of value because it facilitated a coupled field solution of the major internal transport mechanisms within the system utilising realistic transportation phenomena numerical formulations, and a limited set of boundary condition assumptions including cathode current, external cooling film coefficients and external bulk fluid temperatures. Visualisation of the flow and temperature patterns in the furnace provided designers with a tool to gain deeper insight into the mechanisms that pose challenges for refractory and cooling systems design.

It was reasoned that in a well-designed commercial operation, the primary power of the furnace reports directly to the process without requiring significant indirect heat transfer by convection and radiation via the walls of the vessel. The raw material thereby acts as a sink to remove the process energy and the balance of the input energy has to be dissipated by the vessel. This is primarily a function of the internal temperature distribution, but is influenced to a lesser extent by the heat transfer mechanisms developing in the freeboard, slag and metal.

It was however recognised that the arc velocity and temperature profiles at heat loss power levels would differ significantly from those at full power because the arc characteristics are determined primarily by the current conducted by the plasma. The heat loss model was previously used only for comparative evaluation of design and operating changes, but without a capability to account for process energy dissipation, could not be used as a full design tool. The cycle of the development reported in this paper focused on extending the capability of the application software in the following key areas:

- The extension of cell definition parameters and solution routines to enable surface to gas, gas to gas and gas to surface radiation heat transfer within the freeboard area of the furnace to be more accurately described.
- Realistic energy absorption modelling capabilities based on published material properties of state and thermodynamic data of process reaction enthalpies, whilst avoiding complex assumptions and additional boundary conditions.

## 2 APPROACH METHODOLOGY

### *Radiation*

This mechanism is important to represent the effect of radiation attenuation by dust clouds in the freeboard. The discrete beam solution of gas to gas, and surface to gas radiation heat transfer mechanisms are well published in the literature and does not require detailed discussion in this paper [1,2]. The equations were incorporated into the heat balance modules of the application software, together with additional methods of calculating geometrical parameters required for the description of radiation heat exchange. Special attention was given to formulating an efficient method of numerically determining view factors between cell boundary surfaces using a beam release and interception model. The model is thereby capable of avoiding heat transfer between two surfaces which are screened from one-another by interposing surfaces. As an illustration, certain parts of the roof cannot “see” the arc directly due to screening by the elements associated with the tip of the electrode surface, but exchange energy with the arc via elements on the slag surface.

### *Energy Absorption*

Applications such as Fluent® have capabilities of modelling the theoretical chemical equilibrium conditions of molecular species within the system directly, thereby enabling the heat absorbed or released by the reaction to be accounted for as part of the coupled CFD solution. This is important for modelling phenomena in which reaction kinetics are influenced by velocity, pressure and temperature fields and vice-versa such as combustion.

A review was carried out to assess the dominating coupling mechanisms for electrically powered pyrometallurgical processes, which take place in the liquid state such as the reduction of molten metallic oxides using a suitable reductant such as Carbon, Silicon or Aluminium. The reduction process is endothermic, and energy is also required to melt the raw materials in order to ensure that suitable process conditions are maintained. The process may be simplified by considering discreet stages as detailed below. However, the list is not necessarily a strict sequence as some of the steps may take place simultaneously, change order as the reaction proceeds, or the process temperature is increased.

- Melting of the metallic oxides, accompanied by various changes in the mineralogy of the ore as it is heated.
- Melting of fluxes required to obtain the desired slag chemistry which yields a suitable liquidus temperature, chemical neutrality to the refractory working lining, and viscosity.
- Contact of the oxide in the liquid state with a combination of solid and volatilised / gaseous reductant.
- Chemical conversion of the metallic oxide to metal particles, formation of solid or gaseous by-products, and sub-reactions, which determine the slag chemistry.
- Coalescing and settling of the metallic phases into the metal bath.

Observations of practical DC operations suggest that gaseous by-products (mainly CO and $H_2$ in most commercial operations) evolve at or close to the freeboard-slag surface at ambient pressures. The temperature of the gas is similar to that of the slag. The exclusion of oxygen in enclosed furnaces prevents further combustion of CO to $CO_2$, thereby making it unnecessary to model this influence on the overall system. The gas evolution gives rise to a net up-flow velocity towards the off gas port, but these are of secondary importance compared to the velocities generated by forced convection of the arc in the freeboard. It is also difficult to model phase change phenomena in CFD whilst simultaneously satisfying conservation of mass in the different zones. The velocities in the slag at the freeboard influence the mixing and distribution of the raw materials, but it is considered unlikely that the slag velocity will have a significant influence on reaction kinetics.

The foregoing was used to conclude that the energy absorbed by the process is primarily coupled to the process temperature. More-over, practical observation and experience with the heat loss model has demonstrated that temperature fields in the slag and metal zones are virtually uniform, and in the superheated temperature ranges of the materials considered. This means that it is not important to accurately quantify the temperature-enthalpy path followed by the materials during the conversion. It is rather necessary to accurately quantify the total energy required to bring the material into the operating temperature range, together with the energy change over a narrow range in the superheated region, which in turn is mostly dominated by the specific heat of the liquid.

***Approach Methodology***

The methodology adopted was to quantify the enthalpy-temperature dependency external to the CFD analysis using a thermodynamic database such as Fact-Sage® [3]. A representation of the temperature enthalpy relationship for a typical recipe required to produce Ferrochrome is shown in Appendix A. The enthalpy includes provision for sensible heating to melting point, calcination of fluxes, latent heat of fusion (melting), reaction energy, and superheating of the slag and metal phases. This relationship is then approximated using equations encoded into a user subroutine, and applied to cells in a specified region of the slag and metal bath as sink terms in which energy generated by source terms (magnetic and resistive heating) elsewhere in the model is extracted.

The model is numerically solved in a pseudo-time dependent analysis, as described in the previous INFACON X paper [4]. The various mechanisms are switched on and ramped up sequentially to the boundary condition values, and relaxation factors adjusted to ensure that the solution remains sufficiently stable and converges. At each iteration after the energy absorption mechanism is activated, the energy balance in specified cells is assessed using the energy absorption model based on the current temperatures in those cells. The solution is finally solved in steady state when all boundary conditions have reached their terminal values, and all fields (temperature, pressure, velocity, current distribution and electrical potential distribution) are close to convergence. Whilst it has been stated that the shape of the temperature-enthalpy curve is not important outside of the estimated target temperature ranges, the equations developed should not incorporate significant discontinuities, which promote numerical instability and increase the computations required to produce a converged solution.

This methodology is further justified by the following considerations:

- The CFD analysis is complex and involves simultaneous solution of strongly non-linear functions. Significant numbers of computations are required to produce a converged solution. The computational effort is also a function of the modelling detail and mesh refinement. Whilst non-coupled solutions are generally not favoured because of their restrictive assumptions and need to transfer data between sequential solutions in different applications, it was felt that the simplified energy absorption model enables the additional computational effort required for modelling chemical reaction phenomena to rather be utilised for mesh refinement. This has been found to improve solution accuracy, particularly in areas of severe field gradients such as the arc region.
- A direct chemical reaction solution still requires assumptions to be made as to the area in which the reactions take place, in as much as the heat absorption model requires assumptions to be made as to where the heat is absorbed. The chemical model is also limited by the assumptions required to reconcile the mass flux between the slag and metal phases simultaneously with a converged mass and energy balance, as well as quantifying the temperature at which the metal is reduced, and the interaction between the two phases during settling and disengagement.
- The CFD analysis is essentially steady state, but a comprehensive mathematical description is required to allow for a steady accumulation of material in the bath to feed the chemical reaction, as most pyrometallurgical process are operated in batch mode. As stated earlier, it is difficult to model this type of process in CFD simultaneously with implicit conservation of mass requirements. In the model presented, the effect of steady state material flow into the system and the subsequent reactions are modelled as continuous heat removal via user defined sink terms and the relatively small effect of changes in inventory has been neglected to simplify the analysis.

## 3. NUMERICAL MODEL

A benchmark model with typical geometry and features of a 40 MW DC Arc Furnace used for the production of Ferrochrome was generated. The details of the model are shown in Fig 1 below. The model represents a 5 degree slice of the furnace utilising the cyclical boundary condition features of Flo++® to simulate the axis-symmetric nature of the system. The model was designed to demonstrate the variety of vessel cooling systems that can be solved for conjugate heat transfer using film coefficients and transport phenomena established simultaneously with the CFD modelling.

The anode was modelled as a doughnut by applying a zero electrical potential boundary condition to this area at the interface between the anode refractory material and the metal bath. The cathode (electrode) vertical surface was adiabatic (zero thermal gradient). The boundary conditions at the cathode tip surface containing the arc attachment zone included a specified temperature and current density distribution in accordance with the work of J. Alexis [5]. The integral of the current distribution over the boundary area was set to equal the applied current. All interfaces between adjacent fluid regions, and solid-fluid regions are modelled as conducting baffles, as described in more detail in the INFACON X paper [4]. The boundary conditions at the outside surfaces of refractory walls or copper cooler plates are free or forced convection systems as applicable to each distinct region, with an associated cooling fluid temperature of 25°C. An emmissivity of 0.8 was applied to all surfaces enclosing the freeboard region.

The plate (ledge) type copper coolers are shown as continuous rings. The actual system is comprised of a sector of plate, sector of refractory, sector of plate arranged in a symmetrical fashion at every cooler level. In the vertical direction, the position of vertically adjacent copper plates are staggered to even out the effect of

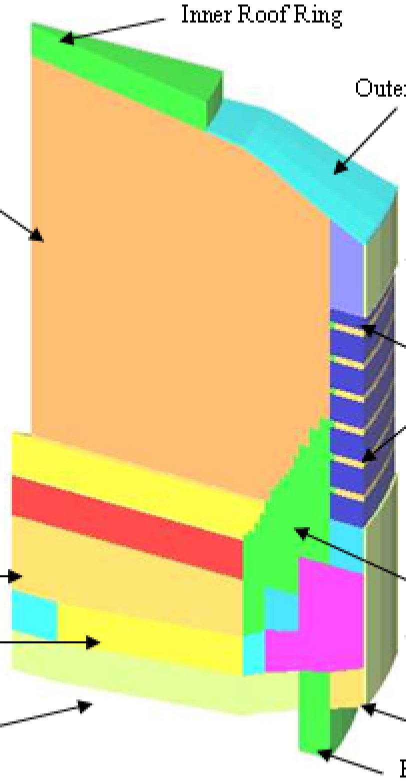


*Figure 1: Composite layers of the numerical mesh for a typical single-electrode DC Arc Furnace*

discreet locations of intense cooling. It was not possible to model this arrangement with an axis-symmetric approximation without significantly increasing the size of the model. The approximation was then modelled by reducing the conductivity of the copper in the ratio of copper to refractory hot face area to simulate the correct heat extraction capability of the refractory cooling system. This resulted in loss of predicted circumferential variation in velocity and temperature fields, but the CFD results were not anticipated to be significantly affected because of domination by radiation, and the modelling of refractory / feed material accretions to the hot face of the copper coolers.

The key model parameters were:

- Electrode diameter 610 mm.
- Hearth internal diameter 9300 mm.
- Arc length 660 mm.

Temperature and heat flux boundary conditions include:

- Fixed electrode tip temperature of 4300 K, corresponding to the sublimation temperature of carbon (graphite).
- Vertical cathode surface temperature of 1923 K during the initial stages of the simulation, followed by adiabatic conditions in the steady state analysis, which was found necessary to promote numerical stability in this zone.

The following additional general assumptions were made for the development of the model:

- Absorption of radiation energy by the plasma within a radius of 1700 mm from the arc centreline was excluded to avoid unrealistic electrical potential fields from developing.

- No provision was made to model the arc attachment zone depression due to arc thrust on the slag surface.
- The copper collector plate located between the bottom of the electrically conductive refractory matrix and the anode support plate was not incorporated in the model, as its contribution to thermal resistance is negligible.
- The furnace shell was not modelled, as the thermal resistance of the steel is negligible compared to the refractory thermal resistance.
- Inner roof ring was constructed of material with properties similar to Verocast 50 FG refractory (450 mm thick).
- Outer roof ring was constructed of material with properties similar to VR60 refractory (40 mm thick)
- Operation with banks of partially reacted raw material at the sidewalls to assess the protection capability of side feeding systems. This area was modelled as a series of horizontal cutbacks instead of a continuous slope to avoid numerical instability produced by transition between wedge shaped elements and brick elements. Some detail of the flow patterns in this area was lost due to disturbances caused by the discreet discontinuities of the surface.
- Heat absorption area restricted to the first third of the slag and metal volumes to simulate the effect of highest reaction kinetics in the superheated slag region below the arc attachment zone.

In the energy absorption model, the power density ($MW/m^3$) in the slag and metal has been selected so that when the power input approximates that which would be supplied to a vessel of this size, the power dissipated by absorption and losses to ambient / cooling systems corresponds to the target process temperature. Although this appears to ensure an obvious result, it actually facilitates modelling of the power to feed ratio algorithm used in practice. In a commercial operation, one of the primary control set points is power input. This is combined with the measured heat loss characteristic of the vessel, and the adjusted Specific Energy Requirements (SER) of the process (and any heat-loss catch-up parameters following a significant shutdown) are utilised to determine the corresponding raw material feed rate of the particular recipe. In addition, the power to feed ratio (or SER) is further adjusted iteratively after each tap to ensure that the target slag and metal tapping temperatures are being maintained.

An explanation is required for the need to extract heat in both the slag and metal regions. In the heat loss model, some depression of the metal temperature was observed below that of the slag. Although this was generally less than that observed in practice, it was assumed that the differential was caused by the slag thermally insulating the metal from heating by the arc jet. During the development of the heat absorption model, it was noted that the metal temperature tended towards the slag temperature as the arc power was increased. After some trial runs were carried out with energy absorption applied to different regions within the slag bath and heat balances checked, it was noted that the high power arc induces sufficient stirring in the slag so that the energy lost by the metal is balanced by the convective heat transfer to the refractory in contact with the metal. This low temperature differential is contrary to that observed in practice, and it is therefore assumed that an additional mechanism is involved in the formation and separation of the metallic phase.

The raw materials melt over a temperature range dependent on the ore chemistry, mineralogy, calcining and chemical reactions with the fluxes. The reduction takes place over a range of temperatures as the metal oxides are progressively exposed to the reductant. It is assumed that this results in the formation of a portion of metal droplets below the ultimate temperature of the slag, which then settle through the slag layer with insufficient retention to be fully heated by the relatively viscous surrounding material. Whilst the heat convected by the slag to the metal is sufficient to support heat losses to the relatively insulating lower hearth, it is probably insufficient to heat the metal back to the slag temperature. As an approximation to this phenomenon, the heat extraction rate applied to the metal is similar to:

Metal production rate* liquid metal specific heat* (slag temp – (metal liquidus temp + a nominal superheat margin))

The process energy absorbed by the slag has been reduced by this quantity so that the total energy absorbed corresponds to feed rates encountered in practice.

## 4. DISCUSSION OF THE NUMERICAL RESULTS

CFD solutions were obtained for two arc current boundary conditions applied to the same furnace geometry and construction as detailed below. The two sets of results files enabled the effect of arc power on the velocity and temperature profiles throughout the system to be assessed.

- Heat loss conditions: The current was adjusted to 13 kA, at which the target slag process temperature of 1650°C was achieved. This was also the benchmark case to assess the effect of the additional radiation transport models incorporated into the application software. At this condition, the heat loss to the ambient and water cooled systems corresponded to 5.7 MW, which was similar to earlier work on a furnace of the same inventory and internal dimensions.
- Process energy absorption model: Sink terms were quantified for the slag and metal zones, and the current adjusted to 53 kA, at which the same slag temperature as the heat loss model was achieved. The process energy absorbed was found to be 39 MW, whilst the heat loss of the vessel increased to 7 MW.

The distribution of heat losses in the different zones of the model under the two boundary conditions are summarised in Table 1 below.

**Table 1: Heat extracted through the refractories and percentage contribution for a full model (refer to Figure 1 for region descriptions)**

| **Region of the Model** (refer to Figure 1) | **Energy flow at 6 MW applied power** | | **Energy flow at 46 MW applied power** | |
|---|---|---|---|---|
| | MW | % of Total | MW | % of Total |
| MAG B1 between copper plates | -0.09 | 1.65 | -0.12 | 1.67 |
| VR60 skewback next to pillar | -0.01 | 0.17 | -0.01 | 0.15 |
| VR60 Outer roof ring | -3.07 | 53.74 | -3.84 | 54.66 |
| Copper- & refractory combo | -1.58 | 27.77 | -1.98 | 28.13 |
| Air-cooled hearth | -0.37 | 6.43 | -0.38 | 5.39 |
| Inner roof ring | -0.18 | 3.11 | -0.22 | 3.13 |
| Permasit Pillar | -0.01 | 0.19 | -0.01 | 0.16 |
| Sigri Paste (free convection) | 0.00 | 0.01 | 0.00 | 0.01 |
| Sigri Paste (water-cooling) | -0.40 | 6.93 | -0.47 | 6.69 |
| **TOTAL** | **-5.71** | **100.00** | **-7.03** | **100.00** |

Note that heat is predominantly lost from the outer roof ring and refractory cooling system in both models.

The temperature and velocity fields in the arc region for the two different currents are shown in Fig 2 to Fig 5 below.

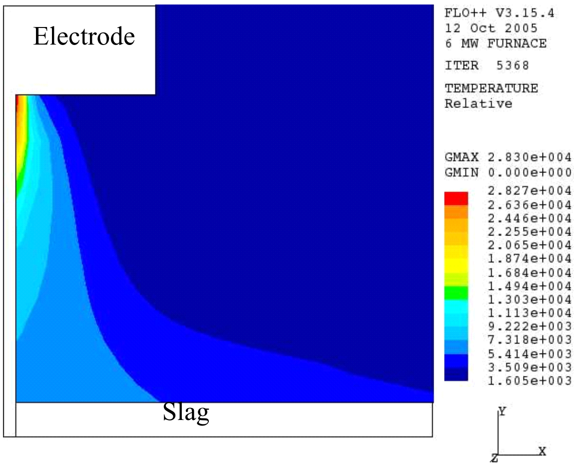


*Figure 2: Temperature contour distribution in the arc region [P = 6 MW]*

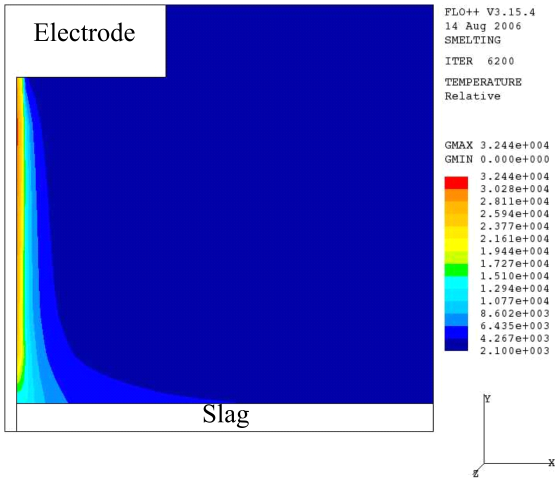


*Figure 3: Temperature contour distribution in the arc region [P = 46 MW]*

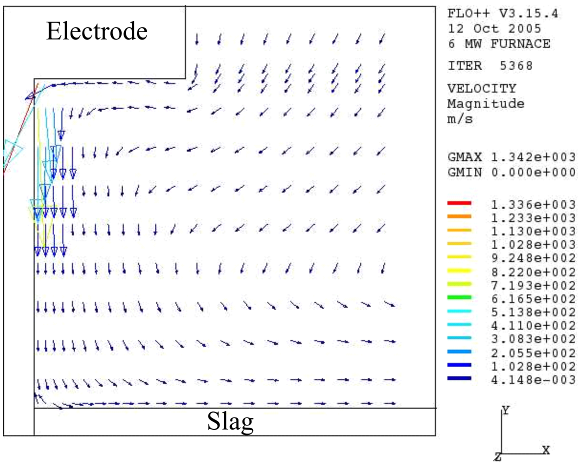


*Figure 4: Velocity vector distribution in the arc region [P = 6 MW]*

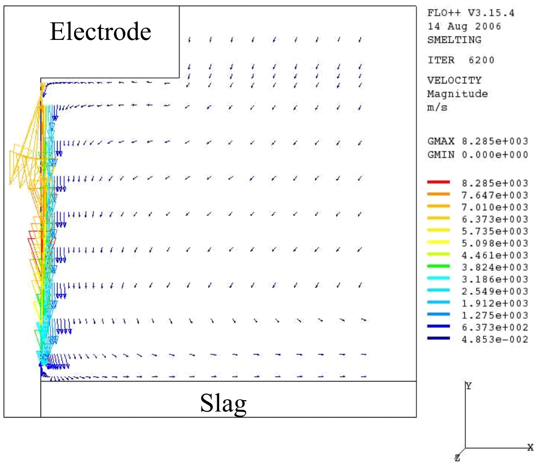


*Figure 5: Velocity vector distribution in the freeboard [P = 46 MW]*

The arc temperature and velocity increase significantly when the arc current is increased from 13 to 53 kA. The velocity increases due to the increased electrical potential through which the plasma ions are accelerated. The temperature increases due to the increase in resistive heating, but not in proportion to the anticipated $P = I^2R$ relationship. This is because the high current arc entrains significantly more gas from the freeboard than the low current arc, which assists in moderating the theoretical arc temperature increase. The increased momentum of the 53 kA arc column is apparent by comparing the temperature contours to those of the 13 kA arc column. The temperature gradient in the 53 kA arc column at the arc attachment zone on the slag surface is significantly greater than the 13 kA arc column, implying that the high current plasma is able to reach the slag surface with far less de-acceleration by entrained freeboard gases.

The increase in heat loss from the vessel is caused by the increase in the predicted arc and freeboard temperature distribution, due to increased radiation and convection from the arc. The temperature of the freeboard for the 53 kA arc is higher than observed in practice, where the measured temperature is close to that of the slag surface. This model does not take into account the heat absorbed by the raw material as it falls through the freeboard, as well as the radiation attenuation by the significant cloud of dust caught up in the circulating freeboard gases, which is the primary cause of the temperature over-prediction.

The temperature and velocity fields in the slag and metal for the two different currents are shown in Fig 6 to Fig 13 below.

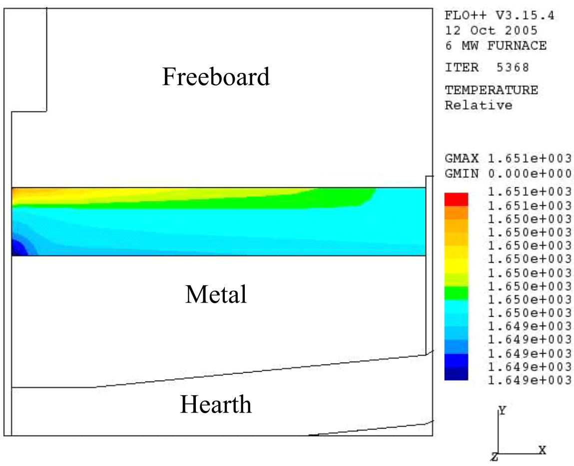


*Figure 6: Temperature contour distribution in the slag bath [P = 6 MW]*

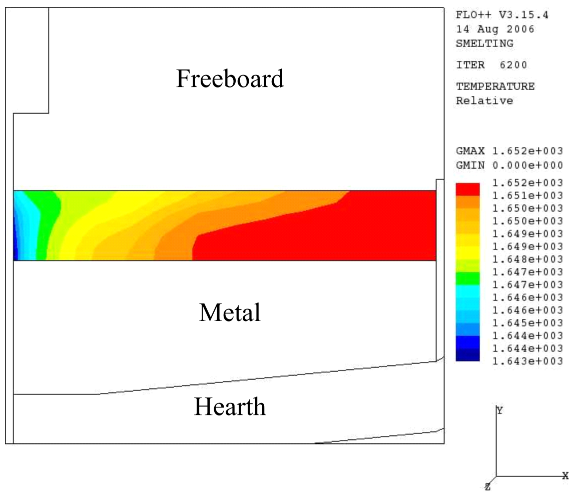


*Figure 7: Temperature contour distribution in the slag bath [P = 46 MW]*

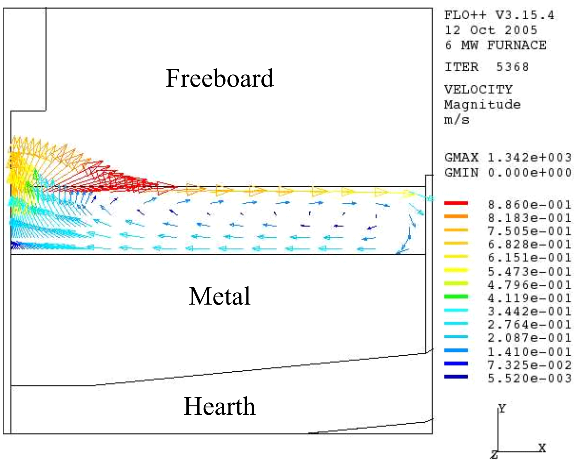


*Figure 8: Velocity vector distribution in the slag bath [P = 6 MW]*

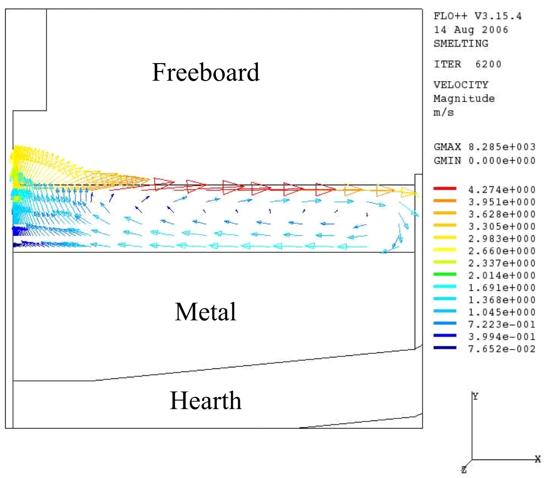


*Figure 9: Velocity vector distribution in the slag bath [P = 46 MW]*

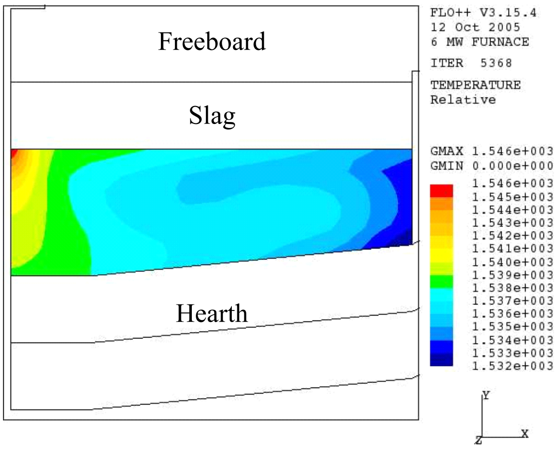


*Figure 10: Temperature contour distribution in the metal bath [P = 6 MW]*

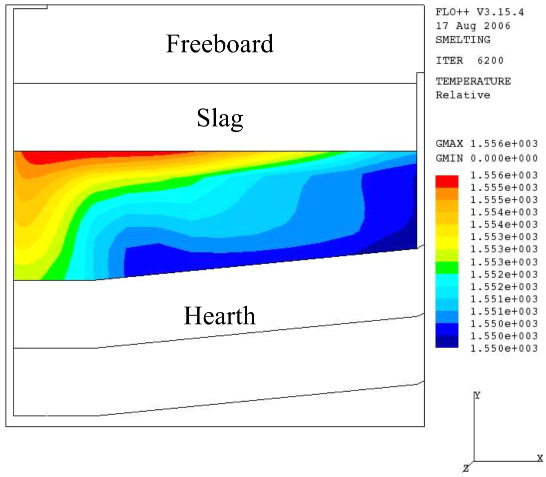


*Figure 11: Temperature contour distribution in the metal bath [P = 46 MW]*

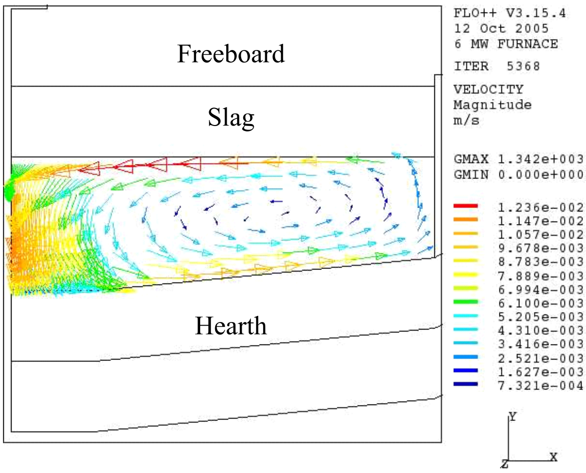


*Figure 12: Velocity vector distribution in the metal bath [P = 6 MW]*

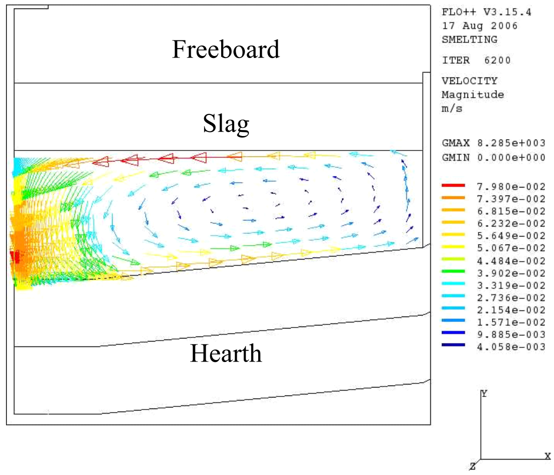


*Figure 13: Velocity vector distribution in the metal bath [P = 46 MW]*

The velocity in the slag increases significantly under the shear coupling with the high velocities of the 53 kA arc. This is able to distort the temperature gradient from virtually vertical disposed in the case of the 13 kA arc to horizontally disposed in the 53 kA condition, implying greater convection of heat towards the side wall. The total gradient across the slag increases from approximately 2°C to 9°C demonstrating both the effect of increased convection, and the heat absorption model applied to the inner third of the slag volume.

The increased shear coupling between the 53 kA arc and the slag extends into the metal region, where the forced convection velocity in the metal increases in the same proportion as in the slag velocities when compared to the 13 kA condition. The temperature gradients in the metal zone of the 53 kA arc model established in the first 1/3rd radius of the metal bath support the heat flow required to satisfy the sink terms specified in this region. The sink term is sufficient to obtain the same temperature difference between the slag and metal in the 53 kA, vigorously stirred model as that in the lower velocity, 13 kA model.

## 5. CONCLUSIONS

The amount of information available to the designer from the arc-bath model has increased due to the incorporation and refinement of additional transport mechanisms, and development of a tool for assessing the effect of energy absorbed by the pyrometallurgical process. It is now possible to model the arc at full power, giving greater insight into its effect on the temperature and velocity fields in the freeboard, slag and metal regions of the furnace. Although the number of simultaneous non-linear phenomena incorporated into the model has increased, the solution algorithms developed have been demonstrated to be capable of maintaining numerical stability and convergence of the simulation.

The full powered arc increases the freeboard temperatures beyond those typically observed in practice, and the associated heat losses beyond those predicted by the heat loss model. Additional energy absorption zones are required to account for energy absorbed by the raw material as it falls through the freeboard, as well as banks of partially reacted raw materials adjacent to the furnace walls. Reduced absorptivity of the dust-laden gas circulating in the freeboard is required to attenuate the radiation transferred to the vessel walls.

Modelling the increased stirring in the bath by a full power arc under energy absorption conditions and assessing the temperature difference between the slag and metal has highlighted that the slag and metal cannot be modelled as two discreet regions, and additional transport phenomena are present due to the mass and energy fluxes of the metal between the two phases. A simplified model has been proposed to account for this, and demonstrated to produce similar temperature differentials between the slag and metal to those observed in practice

## 6. FUTURE DEVELOPMENTS

The energy absorption model has enabled full-scale arcs to be modelled without obtaining unrealistic field gradients. However, it is possible to modify the results by changing the position, zone extent and quantities of heat extracted, which is not desirable in a predictive design tool. Further work is required to rationalise the selection of these boundary conditions to ensure that they are consistent both from one model to another and with the physical situation being simulated.

In addition, the following issues will be addressed during the next phase of the model development:

- Influence of slag velocity on metallic droplet separation, and investigation of the transportation mechanisms between the slag and metal.
- Effect of varying the absorptivity of the gas cloud containing fine material in the freeboard.
- Arc-bath interaction to establish the equilibrium shape of the arc depression zone.
- Validation of the model from experimental results and field measurements.
- Dynamic, time dependant arc model.

## REFERENCES

[1] Lockwood, F.C., and Shah, N.G., “A new radiation solution method for incorporation in general combustion prediction procedures”, Proc. 18$^{th}$ Symposium (International) on Combustion, Combustion Institute, 1981.

[2] STAR-CD Version 3.10A Methodology Manual, 1999, Chapter 9, pp. 1-9.

[3] Fact-Sage® Software, Internet website: www.factsage.com.

[4] Henning, B., Shapiro, M., and le Grange, L., “DC Furnace containment vessel design using Computational Fluid Dynamics”, Proceedings of the Tenth International Ferroalloys Congress, 1 – 4 February 2004, pp. 565-574.

[5] Alexis, J., Ramirez, M., Trapaga, G., and Jönsson, P., “Modelling of a DC Electric Arc Furnace – Heat Transfer from the Arc”, ISIJ International 2000, vol. 40, no. 11, pp. 1089-1097.

## APPENDIX - A

Enthalpy - Temperature Curve
Typical RSA FeCr Production Recipe

| Feed Material Description | Mass (g) |
|---|---|
| Chromite | 1000 |
| Quartzite | 107 |
| Dolomite | 215 |
| Coke | 250 |

Reactions: $Fe_2O_3 + 3C = 2Fe + 3CO$
$Cr_2O_3 + 3C = 2Cr + 3CO$

Feed temp (C) 25

Total Enthalpy of material predicted by FactSage (r)
(including energy of reaction)

| Equil'm temp | Enthalpy |
|---|---|
| T(C) | Delta_H(kJ) |
| | |
| 1200 | 11346 |
| 1205 | 11465 |
| 1224 | 12166 |
| 1245 | 12647 |
| 1250 | 12663 |
| 1300 | 12814 |
| 1350 | 12970 |
| 1400 | 13135 |
| 1450 | 13311 |
| 1477 | 13414 |
| 1500 | 13484 |
| 1550 | 13634 |
| 1600 | 13786 |
| 1650 | 13943 |
| 1700 | 14113 |
| 1750 | 14309 |
| 1752 | 14316 |
| 1800 | 14487 |
| 1850 | 14691 |
| 1900 | 14925 |
| 1950 | 15187 |
| 2000 | 15477 |